Catalysis Today 143 (2009) 274–281

Contents lists available at ScienceDirect

Catalysis Today

journal homepage: www.elsevier.com/locate/cattod

Photocatalytic behaviour of Bi_2MO_6 polymetalates for rhodamine B degradation

C. Belver [a,*], C. Adán [b], M. Fernández-García [b]

[a] Instituto de Ciencia de Materiales de Madrid, CSIC, Campus Cantoblanco, C/ Sor Juana Ines de la Cruz 3, E-28049 Madrid, Spain
[b] Instituto de Catálisis y Petroleoquímica, CSIC, Campus Cantoblanco, E-28049 Madrid, Spain

ARTICLE INFO

Article history:
Available online 30 October 2008

Keywords:
Polymetalates
Aurivillius structure
Photocatalysis
RhB degradation

ABSTRACT

Bi_2MO_6 (M = W or Mo) have been successfully synthesized using the citrate complex method. The samples were characterized by X-ray diffraction, Brunauer–Emmet–Teller surface area and UV–vis spectroscopy. The solids crystallized in the orthorhombic Aurivillius-type structure and display optimum light absorption properties to be used as photocatalysts. The photoactivity power of the samples was investigated systematically using the rhodamine B degradation under different irradiation wavelengths. The behaviour of the solids and the photodegradation mechanism was studied as a function of the irradiation light (UV or visible) employed. Direct solar light was also employed as irradiation source showing that this type of structures could drive to a plausible strategy for developing finest photocatalyst to degrade wastewaters by using solar light.

1. Introduction

In the past decades, the photocatalytic technology has attracted much attention and been widely studied with the final aim of efficiently eliminating the undesired chemical substances for environmental conservation [1,2]. The photocatalytic materials have mainly focused on TiO_2 semiconductor because of their high reactivity, low cost and environmentally friendly features [3,4]. Nevertheless, the TiO_2 needs UV light irradiation to produce the electronic transition responsible to its photoactivity because of its large band gap of 3.2 eV. The ultraviolet radiation constitutes less that 4% of whole energy of incoming solar spectrum, while the visible light is more than 50%. Hence, effective utilization of the solar energy appears nowadays as the main aim of photochemical researchers [5,6]. In this sense, many efforts have been dedicated to modify the TiO_2 with the goal to shift the spectral response of TiO_2 into the visible region ($380\ nm < \lambda < 750\ nm$) and improve its photocatalytic performances. Some of the most feasible modifications are doping (cationic or anionic), metal deposition and surface sensitization [4,7,8].

On the other hand, in recent years many efforts have been paid to develop new type of photocatalytic materials active under sunlight mainly based on oxide semiconductors [5,9,10]. The strategies described to enhance the visible light absorption of the oxide semiconductors are focused in the modification of their band gap [11]. In general, these oxides are based on metal cations with d^0 or d^{10} configurations. The conduction bands (CB) are usually formed by the empty orbitals of the metal cations, whereas the valence band (VB) is based on O 2p orbitals. A way to modify the band gap consists of creating an electron donor level between the VB and CB, as occurred during the metal doping of TiO_2 [6] or the continuous modification of the conduction band for high levels of doping cations [12]. Another way to the band gap modification could be the formation of new VB employing elements with orbitals other than O 2p. In this sense different metalates, described as $A_xB_yO_z$, have been studied as optimal materials for visible light absorption [13,14]. The development of these materials is influenced by their photocatalytic applications, being photodegradation reactions and water splitting the most common [15,16].

The presence of cations such as Bi^{3+}, In^{3+}, Sn^{2+} (s^2 configuration) or Ag^+ (d^{10} configuration) in an oxide system manages to elevate the valence band by means of the combination of their respective orbitals with the O 2p orbital from the oxygen, narrowing the band gap of the semiconductor. In this way, oxides such as $BiVO_4$, $AgVO_x$, $CaBi_2O_4$, $InMO_4$ (M = V, Nb, Ta), Bi_2WO_6 or MIn_2O_4 (M = Ca, Sr, Ba) have been described as effective photocatalysts for contaminant degradation [17–22]. The conducting properties of these materials mainly depend on their electronic properties, as an example it has been reported that the introduction of s orbital components increases the charge mobility, and, at the same time, tunes the relative positions of CB and VB for $InMO_4$ (M = V, Nb, Ta) and $BiVO_4$ systems [23,24]. By other side, the structural properties of these materials are also relevant. The crystallization on complex

* Corresponding author. Tel.: +34 91 334 9000; fax: +34 91 372 0623.
E-mail address: cbelver@icmm.csic.es (C. Belver).

0920-5861/$ – see front matter © 2008 Elsevier B.V. All rights reserved.
doi:10.1016/j.cattod.2008.09.011

structures, such as perovskites, scheelites or spinels, where chains or layers constituted by MO_6 octahedron are formed, favours the formation of a narrow conduction band and the delocalization of the charge carriers [22,25]. As occurred in the case of TiO_2, the photoresponse of these materials could be enhanced by the doping process choosing as dopants metal cations [20,26] or, even, some anions as nitrogen [27]. Nevertheless, these materials have some disadvantages, such as their low surface area and their high particle sizes, mainly caused by the synthesis method usually employed that requires treatments at high temperature. By this reason, important efforts are being performed to optimize the properties of these metalates in order to improve their photo-efficiency under visible light.

Recently, different authors have reported the preparation of bismuth tungsten oxides (Aurivillius structure), with optimum optical properties for photocatalytic purposes, through synthetic procedures based on soft chemical, such as complex organic precursors; microwave-assisted synthesis; mild hydrothermal process or films formation [28–31]. In the present work, the procedure based on citrate complex synthesis, also called Pechini method, has been followed in order to obtain the series of *Aurivillius* Bi_2WO_6 and Bi_2MoO_6 oxides with optimum structural and optical properties. The successful synthesis of these materials will be providing interesting candidates for photocatalytic applications.

2. Experimental

2.1. Synthesis of polymetalates

The polymetalates Bi_2WO_6 and Bi_2MoO_6 were synthesized by the polymeric precursor technique, also known as the citrate complex or Pechini technique [32], which is based on the polymerization of complexes from the metals involved. For the tungsten metalate, stoichiometric molar amounts of $Bi(NO_3)_3{\cdot}5H_2O$ (Sigma–Aldrich, 98%) and $(NH_4)_{10}W_{12}O_{41}{\cdot}5H_2O$ (Riedel-de-Haën, 99.99%) were dissolved, respectively, in a nitric acid solution ($[Bi^{3+}]$ = 0.15 M; nitric acid 1 M) and in a citric acid solution ($[W^{6+}]$ = 0.15 M; ratio citric acid metal 1:6). The resulting solutions were then added together (molar ratio Bi^{3+}/W^{6+} 1:2) and the mixture was stirring for 15 min prior to the addition of ethylene glycol in the ratio ethylene glycol citric acid 10:1 in mole. After sometime of rigorous stirring, the mixture was heating for 170 h, raising the temperature 8 °C each 24 h to reach 85 °C. The brownish resin obtained after this time was subsequently calcined for 10 h at 600 °C with a 1 °C/min heating rate, resulting in a light yellow solid called Bi_2WO_6. The molybdenum metalate was synthesizing in the same way. In this case, $(NH_4)_6Mo_7O_{24}{\cdot}4H_2O$ (Riedel-de-Haën, 99%) was employed as molybdenum source, introducing the stoichiometric amount in the citric acid solution described before. The subsequent thermal treatment yields to a yellow solid named Bi_2MoO_6. All chemicals were reagent grade quality and used without further purification. Deionised and doubly distilled water were used throughout this study.

2.2. Characterization of the solids

Powder X-ray diffraction (PXRD) patterns were registered between 2° and 80° (2θ) with a scanning velocity of 1.5°/min by using a Seifert diffractometer using Ni-filtered Cu Kα radiation (λ = 0.15418 nm). The structural identification was performed by using the JCPDS cards [33]. Lattice parameters were calculated by fitting and refining the unit cell with the UnitCell program based on regression diagnostics processes [34]. Textural analyses were determined by nitrogen adsorption–desorption isotherms at −196 °C using a Micromeritics apparatus (TriStar 123). The samples were degassed for 24 h at 110 °C. Specific surface area were obtained from the BET method. UV–vis diffuse reflectance spectroscopy experiments were performed with a Shimadzu UV2100 apparatus with a nominal resolution of ca. 2 nm.

2.3. Photocatalytic activity

The catalytic properties of the Bi_2MO_6 solids have been evaluated for the photocatalytic degradation of rhodamine B in an aqueous solution. The experiments were performed at room temperature as follows: 500 mg of catalyst was suspended in a 1000-mL Pyrex glass vessel which contained 25 mg/L of rhodamine B (RhB, Sigma–Aldrich, 95%); under a steady stream of air (100 Ncc/min) throughout the experiment. The photocatalytic reactor consists of a 500-W high pressure Hg lamp (supplied by Helios Italquart) located within a cylindrical refrigerated glass vessel. The lamp is cooled by a Pyrex jacket connected to a water circuit. The light emission range of this lamp is comprised between 260 and 430 nm, with two intense bands centred at 318 and 366 nm and several weaker bands at 270, 303, 310, 410 and 430 nm. The average light intensity was measured with a hand radiometer supplied by Cole Parmel (model VLX3V) which measures at 366 nm fixed wavelength. The resulting intensity for UV–vis experiments was 134 W m^{-2}. The photoreactor was provided with two ports in its top section for sampling the solution and/or flowing air as required. Before illumination, the suspension was stirred in the dark for 30 min to achieve the adsorption counterpoise. Then the suspension was exposed to light irradiation under magnetic stirring for 7 h. At given irradiation time intervals, 10 mL of the suspension were collected and the photocatalyst was removed by filtration using 0.45 μm nylon syringe filters. The filtered solution was analysed both by a Varian Cary 50 Scan UV–vis spectrophotometer, monitoring the absorption peak at 554 nm characteristic of RhB and by a TOC-$V_{CSH/CSN}$ Shimadzu analyser, in order to measure the total organic carbon (TOC) of the solution.

The first experiments were performed employing the total light from the lamp, in order to evaluate the behaviour under UV–vis conditions. After then a cut off filter of polyester (supplied by Edmund Optics) was used to cut off the light below 390 nm to make sure the photoreaction went on under the visible light irradiation. In this case the light intensity at 366 nm decreases to 10 W m^{-2} and only two peaks at 410 and 430 nm in the visible region are going through the filter along to 7.5% of UV radiation. In these experiments the experimental conditions (catalyst amount and dye concentration) are the same that in the UV–vis experiments. Final tests were carrying out under direct solar light to get knowledge about the potential industrial applications. In this case, the Pyrex glass vessel (500 mL with 25 mg/L RhB and 0.5 g/L catalyst) was situated under solar radiation in a non-cloudy sunny day maintaining the magnetic stirring constant for 7 h. Experiments were doing for both catalysts at the same time to compare their activity with solar light. The temperature of both systems was comprised between 24 and 26.5 °C. Various aliquots were extracted at several times, filtered and analysed in the same way described before.

3. Results and discussion

3.1. Preparation and characterization of polymetalates

The polymetalates crystallization was investigated by XRD measurements in order to control the structure and phase formed. Fig. 1 shows the XRD patterns of the Bi_2MO_6 (M = W or Mo) powder samples synthesized.

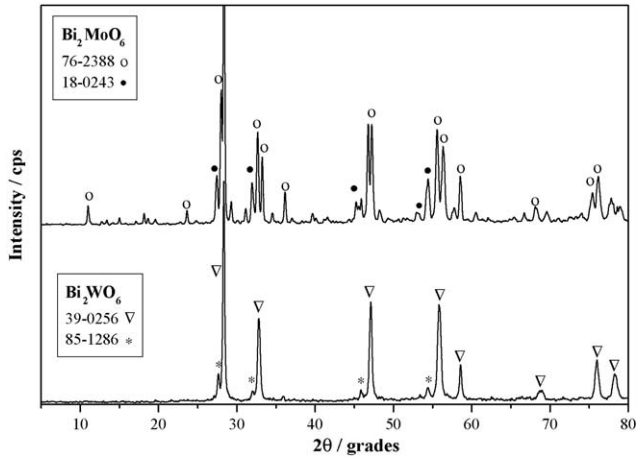

Fig. 1. XRD patterns of the Bi_2MO_6 (M = W or Mo) solids synthesized.

The main diffraction peaks for tungsten polymetalate system are observed at 2θ values: 28.39°, 32.84°, 47.18°, 55.88°, 58.61°, 68.79°, 76.06° and 78.52° which are indexed to orthorhombic ($Pca2_1$) Bi_2WO_6 russellite structure (according to the JCPDS card no. 39-0256) corresponding to the (1 3 1), (2 0 0), (2 0 2), (3 3 1), (2 6 2), (4 0 0), (3 3 3), (2 0 4) planes, respectively. Together with this majority phase appears a small contribution of $Bi_{0.875}W_{0.125}O_{1.6875}$ (JCPDS 85-1286), indicated in Fig. 1. The diffraction pattern from molybdenum polymetalate can be indexed to the isostructural Bi_2MoO_6 koechlinite (JCPDS 76-2388), also an orthorhombic structure ($Pca2_1$) which main diffraction peaks appear at 2θ values: 28.14, 32.69, 33.29, 36.18, 46.79, 47.23, 55.63, 56.37, 58.59, 75.42 and 76.24 corresponding to the following ($h\,k\,l$) planes: (1 3 1), (0 0 2), (0 6 0), (1 5 1), (2 0 2), (2 6 0), (1 3 3), (1 9 1), (2 6 2), (3 3 3), (3 9 1). The presence of traces from other Bi_2MoO_6 phase is evident in the diffraction pattern (Fig. 1); the reflection peaks observed match up with the tetragonal structure described in the 18-0243 JCPDS pattern.

The structure of both bismuth polymetalates is shown in Fig. 2, also known as Aurivillius-type structure [35], and can be described as alternating layers of MO_4^{2-} (M = W or Mo) and $Bi_2O_2^{2+}$ entities lying perpendicular to c direction. The tungsten and molybdenum exhibit a regular octahedral environment where neighbouring octahedra are connected to each other by corner sharing. It was found that this octahedra corner-sharing structure contributed to the photocatalytic activity of these compounds, because of an easy charge delocation within the structure [36]. The coordination polyhedron of the bismuths is more complex but each one is bonded to six oxygens. Bibliographic bond valence calculations described the presence of two crystallographically independent bismuths. For both Bi^{3+} cations the orientations of the lone-pair electrons have been inferred from the 3.0 Å coordination shells and have been found to be non-centrosymmetric. This effect gives rise to the tilting of the tungsten octahedral, yielding a tungsten displacement from the centre of the octahedron by 0.278 Å [37].

The crystal lattice parameters calculated were as follows: a = 5.453 Å, b = 16.364 Å and c = 5.441 Å with a cell volume ca. to 485.574 for Bi_2WO_6, and a = 5.498 Å, b = 16.153 Å and c = 5.483 Å with a cell volume equal to 486.964 for Bi_2MoO_6, which were consistent with the literature data and the diffraction patterns indicated above. The average crystallite size of the polymetalates is 28 nm for Bi_2WO_6 and 26 nm for Bi_2MoO_6, calculated via Scherrer equation from the XRD (1 3 1) peak. The BET surface areas of tungsten and molybdenum polymetalates are 9.9 and 2.2 $m^2\,g^{-1}$, respectively, considerably higher than the surface described by these materials prepared by the conventional solid-state reaction method [38].

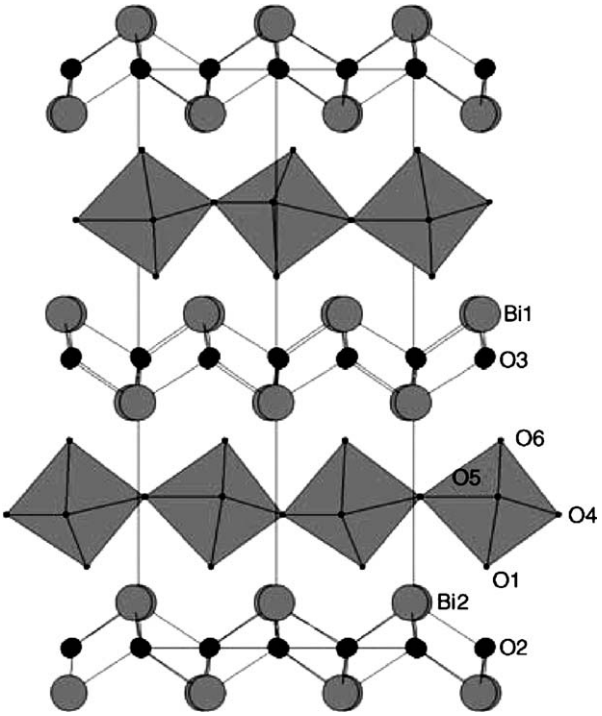

Fig. 2. Crystal structure of the Bi_2MO_6 phase along (1 0 1) direction.

It is well known that upon irradiation a photoinduction process would take place in a semiconductor. This process consists in the migration of one valence band electron to the conduction band, yielding a hole in this valence band. This electron–hole pair created might undergo charge transfer to adsorbed species on the semiconductor surface leading to a photocatalytic reaction [39]. Thus, a study of the photoabsorption ability of the materials was done using UV–vis DRS, showing the spectra of Bi_2WO_6 and Bi_2MoO_6 in Figs. 3 and 4, respectively. Both samples showed photoabsorption properties from the UV light region to visible light region no longer than 500 nm, which suggests the chance of being photoactive under visible light irradiation. The steeped absorption edge describes for both samples indicated that the visible light absorption is due to the band gap transition instead of the transition induced by impurity levels [40].

For a semiconductor sample, it is possible to determine the optical absorption near the band edge by the equation $\alpha h\nu = A(h\nu - E_g)^{n/2}$ [41], where α, h, ν, E_g, and A are absorption coefficient, Planck

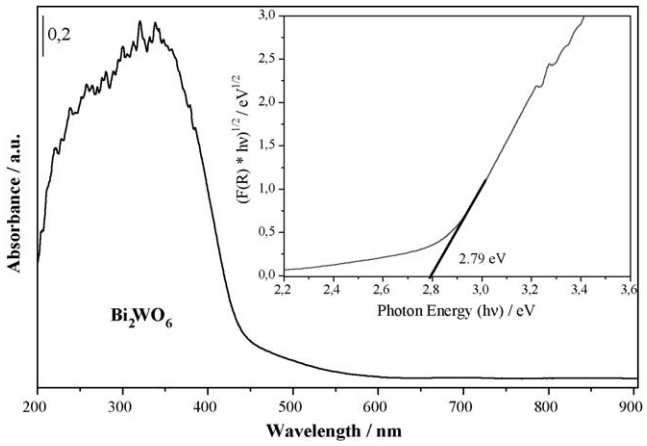

Fig. 3. DR-UV–vis spectrum and Tauc plot of Bi_2WO_6 phase.

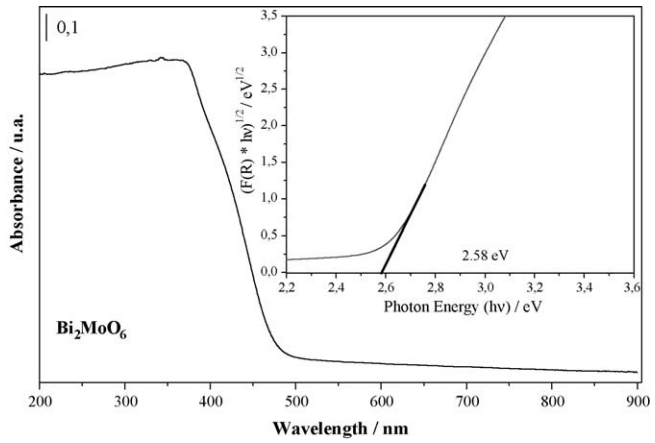

Fig. 4. DR-UV–vis spectrum and Tauc plot of Bi_2MoO_6 phase.

constant, radiation frequency, band gap and a constant, respectively. The *n* value decides the characteristics of the transition in a semiconductor, being 1 or 4, respectively, for a direct or an indirect semiconductor. Assuming the Bi_2MO_6 (M = W or Mo) solids as indirect semiconductors and by taking the square root of both sides from the above equation; it is possible to construct a plot $(\alpha h\nu)^{1/2}$ vs. $h\nu$, also called Tauc plot [42], in order to get an accurate value of the band gap of the solids. For an indirect semiconductor, the plot shows a linear region just above the optical absorption edge. Thus, the extrapolation of this line to the photon energy axis yields the semiconductor band gap value. The Tauc plots for both solids are displayed in Figs. 3 and 4. The energy of the band gap could be thus estimated to 2.79 eV for Bi_2WO_6 and 2.58 eV for Bi_2MoO_6. The colour of both photocatalysts is yellow, as can be expected from their absorption properties.

The electronic structure of Bi_2MO_6 (M = W or Mo) has been reported based on the density functional theory (DFT) calculations [43,44]. The visible light absorption for Bi_2WO_6 was attributed to the transition of the electron from the valence band formed by the hybrid orbital of O 2p and Bi 6s to the conduction band constituted by the W 5d orbital. The hybridization of the bismuth and oxygen levels makes the valence band largely dispersed, which favours the mobility of photo-excitated holes and thus is beneficial for oxidation reactions [22]. By other side, the valence band of Bi_2MoO_6 was composed mainly by O 2p orbitals and the conduction band derived from primary Mo 4d orbitals in MoO_6 octahedra and the secondary Bi 6p orbitals. In this case, it has been described an Aurivillius Bi_2MoO_6 structure with a valence band constituted not only of O 2p orbitals but also of a minor Bi 6s contribution [36]. Both solids possess the corner-sharing structure of MO_6 octahedra as seen in the well-known WO_3 photocatalyst with visible light response. This structure affects the energy gap and the width of the conduction band, which drives the visible light response and controls the photocatalytic performance.

3.2. Photocatalytic degradation of RhB

The photocatalytic behaviour of Bi_2MO_6 (M = W or Mo) materials were evaluated by the photodegradation of rhodamine B (RhB), a dye widely studied as a representative water pollutant [45]. The RhB dissolved in water shows a main absorption band at 550 nm with a shoulder at 516 nm that can be monitored by UV–vis spectroscopy in order to follow its photocatalytic degradation. The activities of both materials are compared under UV–vis light ($\lambda > 260$ nm) and visible light ($\lambda > 390$ nm). Fig. 5(A) and (B) shows time profiles of $\ln[C/C_0]$ vs. irradiation time for both materials under different radiation wavelengths, being C the concentration of RhB at each reaction time and C_0 the initial concentration in the adsorption equilibrium (after 30 min stirring at dark). These plots describe a linear decrease that can be fitted for pseudo-first-order kinetics. Thus, the reaction rate constant (k) determined was 6.3×10^{-3} and 1.7×10^{-3} min^{-1}, respectively, for Bi_2WO_6 and Bi_2MoO_6 under UV–vis radiation and 1.1×10^{-3} and 1.0×10^{-3} min^{-1} under visible light (by using the polyester filter). The Bi_2WO_6 solid exhibited higher photoactivity than Bi_2MoO_6 under UV–vis, as demonstrate the rate constants, nevertheless the difference between both materials diminishes under visible radiation, likely by the low intensity of the radiation. The different performance can be ascribed not only to the different electronic structures but also to the textural properties, due to the lower surface area of the Bi_2MoO_6 catalyst which decreases the reaction place.

The RhB decomposition and TOC values are shown in Fig. 5(C) and (D) for both catalysts using UV–vis and visible irradiation light. Control experiments (not shown) displayed that RhB did not degrade in solid suspension in the dark or when illuminated with visible light at the absence of the catalyst. Nevertheless, UV–vis light alone promoted the photodegradation of RhB yielding to 18% of conversion. However, more than 90% of RhB can be photodegradated by the Bi_2WO_6 when $\lambda > 260$ nm though only 51% is achieved by the Bi_2MoO_6 photocatalyst in 7 h, indicating the removal efficiency of rhodamine B by these catalysts. Nevertheless, the TOC reduction is almost negligible in all cases although RhB spectra show the decrease of its characteristic band, suggesting that the intermediates (not detected by UV–vis spectroscopy) arise during the photochemical process and no mineralization occurs. When $\lambda > 390$ nm, around 36% of RhB is degraded by the Bi_2WO_6 solid after 7 h and 33% by the Bi_2MoO_6 material, quite similar as has been indicated before. Comparing the RhB concentrations and the corresponding reaction rates (Fig. 5) for the different radiations used, is showed that the employment of UV light results in the enhancement of the RhB degradation. Nevertheless, the visible light employed has a radiation intensity considerably lower than UV–vis light, due to the filter cut off.

In order to avoid this effect, the relative photonic efficiency (ξ) was determined according to Serpone [46]. Though ξ was defined as the number of reactant molecules transformed divided by the number of photons at a given wavelength, the author determined that the photon efficiencies could be estimated by the relation between the initial rate of substrate degradation with the rate of incident photons. In this work, the initial RhB degradation was calculated in terms of mol min^{-1} (fitting the experimental data to exponential curves and performing the first derivative of the corresponding curve) and the photon flux was estimated by the radiation intensity measured at 366 nm (being 3.1 and 0.2×10^{-5} einsteins/s for UV–vis and visible conditions, respectively). Thus, the relative photonic efficiencies (ξ) were 7.3×10^{-3} and 1.8×10^{-3}, respectively, for Bi_2WO_6 and Bi_2MoO_6 under UV–vis radiation and 2.6×10^{-2} and 1.2×10^{-2}, under visible light. Once again Bi_2WO_6 solid exhibits more activity than Bi_2MoO_6 under both radiation conditions. Comparing the light source, the resulting ξ data exhibit higher values performing the experiments under visible conditions than under UV–vis irradiation. Although these values are approximate just because only one wavelength component of the light was considered to calculate the photon flux (366 nm), the higher values of the visible experiments indicated that the visible contribution can enhance the activity of the catalyst. If the materials were mainly activated by UV light the photon efficiencies should be analogous for both experiments. The high difference comparing UV–vis and visible experiments suggest that the photodegradation of RhB takes place in a good deal under

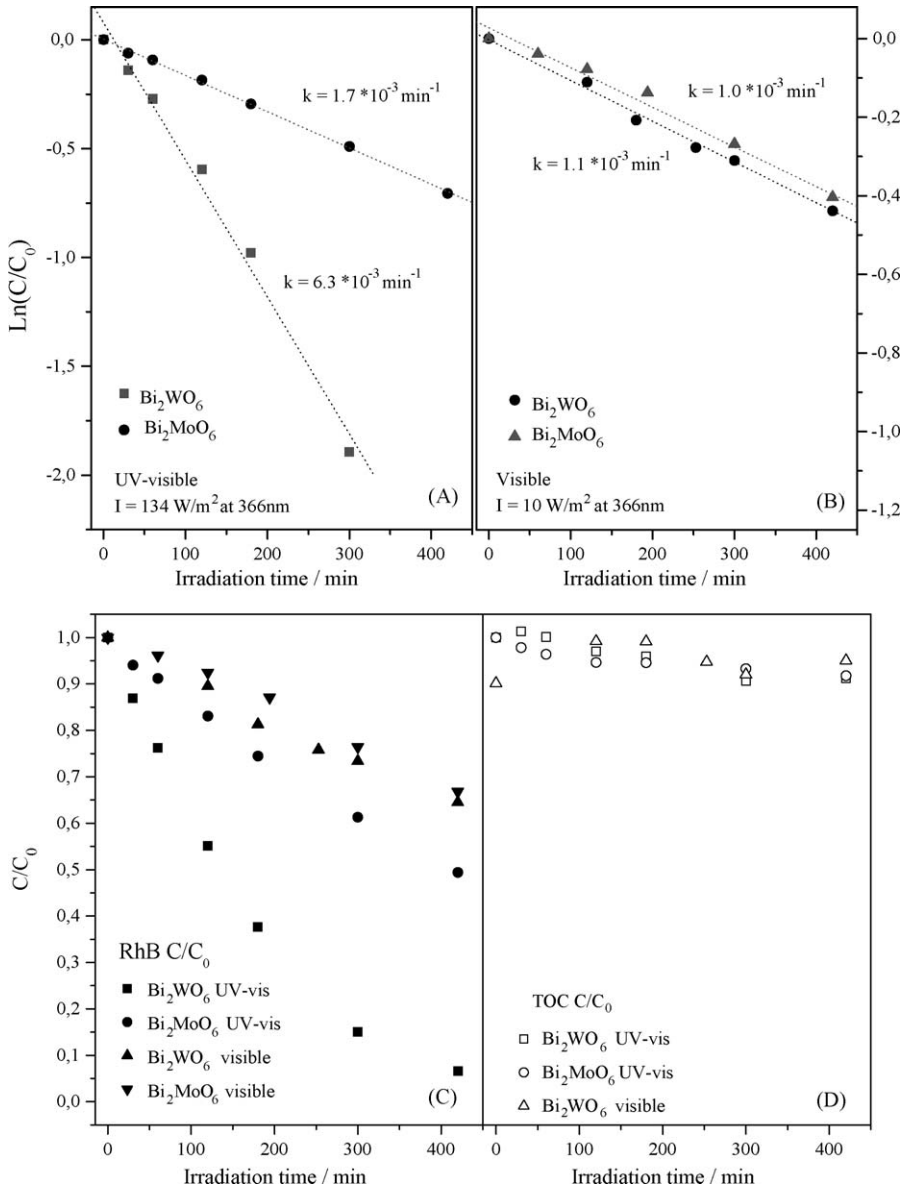

Fig. 5. Photocatalytic degradation of RhB over the Bi_2MO_6 solids under different irradiation wavelengths: (A and B) reaction rates under UV–vis and visible light, respectively and (C and D) RhB C/C_0 concentration and TOC C/C_0 values, respectively, under UV–vis and visible radiation lights. (Bi_2MoO_6 TOC values under visible light not shown, equal to Bi_2WO_6 data.)

visible light ($\lambda > 390$ nm), turning Aurivillius materials into promising photocatalysts.

To further observe the photochemical properties of these materials, the temporal evolutions of the spectral changes that occur during the RhB degradation are shown in Fig. 6, comparing both solids under UV–vis and visible lights. In all cases, the characteristic absorption band from RhB decreases during the irradiation time. For Bi_2WO_6 catalysts (Fig. 6(A)), under UV–vis light the absorption band of RhB decreases dramatically without appearance of other absorption features, indicating that new intermediates or products are not detected in the visible region. The pink colour of the suspension changes gradually and disappears ultimately. For Bi_2MoO_6 (Fig. 6(B)) the RhB band also decreases although not so drastically as the tungsten polymetalate, in any case the absence of other absorption bands is also evident for this catalyst. The maximum absorption decrease and the absence of others bands are in agreement with one of the mechanisms reported in literature for RhB photodegradation, which suggest that the RhB decomposition mainly occurs via the destruction of the aromatic chromophore [47]. Unlike the UV–vis irradiation case, visible radiation light causes the shift of the maximum absorption in addition to the decrease. For the Bi_2WO_6 case there has been a swing from 553.8 to 532.4 nm and from 554 to 548 nm for Bi_2MoO_6 case (Fig. 6(C) and (D)). According to the RhB degradation mechanisms described in the literature, this blue shift in the absorption band of the dye is caused by the N-deethylation of the RhB, yielding to de-ethylated RhB products which light absorption maximum appears at 498 nm [48].

To evaluate the photocatalytic performance of these materials under real conditions, both Bi_2MO_6 (M = W or Mo) photocatalysts were tested for RhB solar photodegradation. The Pyrex photoreactor was placed under direct solar light in a clear sunny day with constant magnetic stirring, taking aliquots at different reaction times. The RhB concentration values, the reaction rates and the temporal evolution of the RhB spectra are shown in Fig. 7 for both solids.

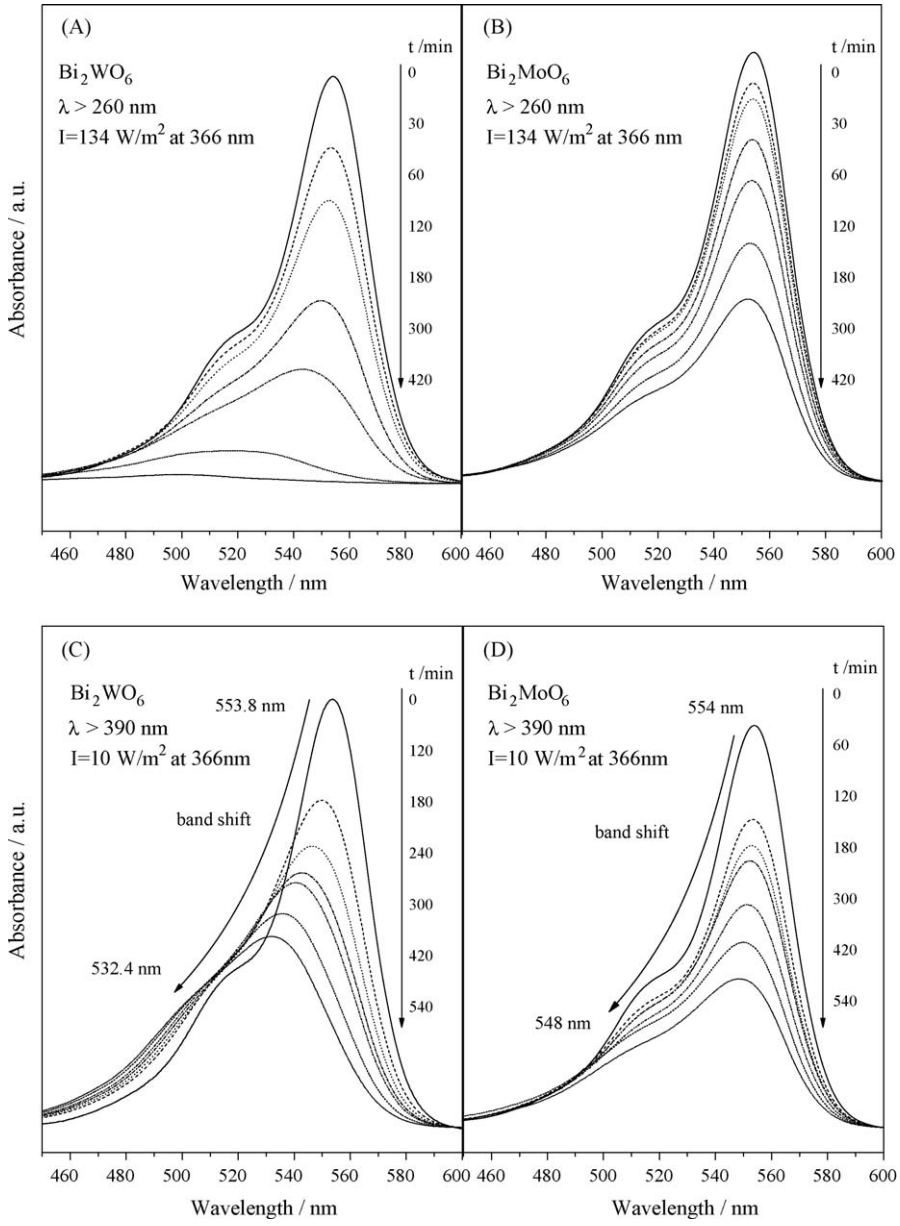

Fig. 6. UV–vis absorption changes of RhB in aqueous suspensions of Bi_2MO_6 as function of the radiation time under different irradiation lights: (A and C) Bi_2WO_6 under UV–vis and visible light and (B and D) Bi_2MoO_6 under UV–vis and visible light.

As occurred in previous experiments, the photoactivity of Bi_2WO_6 solid is higher than the Bi_2MoO_6 activity; this is reflected in the reaction rates calculated, 1.2 and 0.2×10^{-3} min^{-1}, respectively. Such difference parallels the variation between the textural and electronic properties described before. The RhB degradation reaches conversion values of 50% for Bi_2WO_6 after 9 h of irradiation. Nevertheless, the RhB degradation values for Bi_2MoO_6 after 9 h of reaction only reach 15%. Under solar conditions Bi_2WO_6 is clearly more active than Bi_2MoO_6, describing a reaction rate six times higher. However, this high difference was not observed when the experiments were carrying out under visible light. In fact, in that case the reaction rate values were virtually equal (1.1–1.0×10^{-3} min^{-1}). Apparently the activity of the Bi_2MoO_6 under visible conditions was higher than the expected. This different behaviour could be attributed to the contribution of UV radiation emitted by the HELIOS Italquart lamp. An estimated 7.5% of UV radiation passes through the filter and would reach the photocatalyst, being thus a larger contribution than the 4% characteristic of solar radiation. In this way, it could be assumed that this UV contribution enhances the activity of the Bi_2MoO_6 photocatalyst. Therefore, the difference between both photocatalysts was lower under visible light than in the solar experiments.

The UV–vis spectral changes of RhB under sunlight conditions are shown in Fig. 7 for both materials. The maximum of absorption for the Bi_2WO_6 case decreases considerably throughout the irradiation time and shifts also to lower wavelengths (from 553.8 to 538 nm), according to the N-deethylation mechanism cited above [48]. Nevertheless, the shift is less important than in the visible experiment although the rhodamine B conversion is higher. This effect could be related to the ultraviolet contribution of the solar light, as it has been indicated before, which decreases the maximum absorption of the RhB without displaying a shift due to the destruction of the conjugated RhB structure. For Bi_2MoO_6 a slightly decrease of absorption intensity is observed throughout

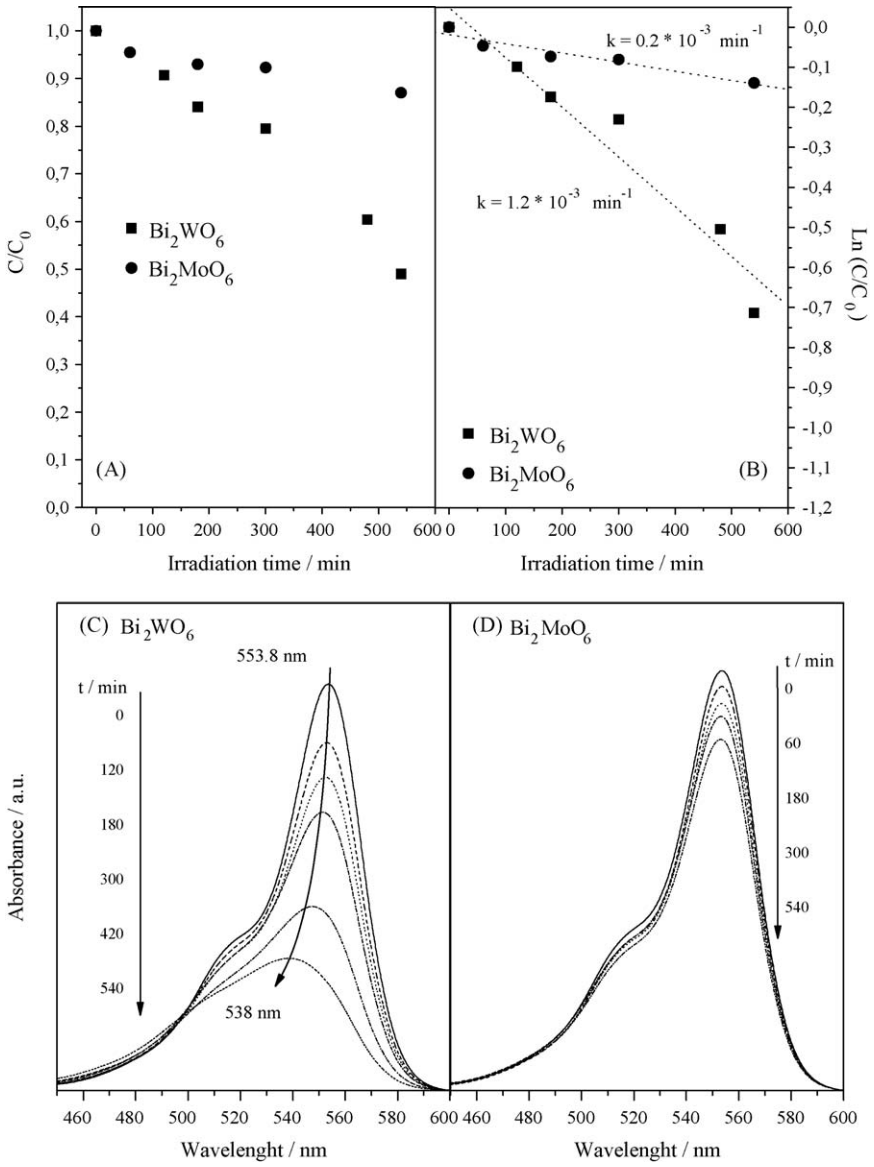

Fig. 7. Solar experiments for Bi_2MO_6 (M = W or Mo) solids: (A) C/C_0 values vs. reaction time; (B) $\ln(C/C_0)$ vs. irradiation time; (C and D) UV–vis absorption changes of RhB in aqueous suspensions of Bi_2WO_6 and Bi_2MoO_6, respectively.

the reaction time, being the behaviour quite similar to that described for visible experiments. Thus, solar irradiation appears as an optimum way to promote the electronic transition in Aurivillius-type materials responsible for the photodegradation of RhB.

4. Conclusions

Bi_2MO_6 (M = W or Mo) catalysts were prepared via the citrate or Pechini method with low crystal sizes, comparing with solid-state reaction conventional method. The optical properties of the materials are optimum for visible light absorption. The photocatalytic experiments revealed that both materials were effective for the RhB decomposition under both UV and visible light although the RhB degradation mechanism seems a function of the radiation wavelength. Bi_2WO_6 appeared as the most active catalyst due to its electronic and textural properties. The experiments run under real solar excitation suggest that Aurivillius bismuth structures could be effective systems for developing optimum photocatalysts to degrade wastewaters using solar light.

Acknowledgements

The authors thank the financial support of this work from Spanish Ministry of Education and Science, Project CTQ2007-60480/BQU. C.B. thanks to CSIC the postdoctoral contract JAE-Doc.

Reference

[1] M.R. Hoffmann, S.T. Martin, W. Choi, D. Bahnemann, Chem. Rev. 95 (1995) 69.
[2] A. Mills, S.-K. Lee, J. Photochem. Photobiol. A 152 (2002) 233.
[3] A. Fujishima, T.N. Rao, D.A. Tryk, J. Photochem. Photobiol. C 1 (2000) 1.
[4] O. Carp, C.L. Huisman, A. Reller, Prog. Solid State Chem. 32 (2004) 33.
[5] H. Arakawa, K. Sayama, Res. Chem. Intermediat. 26 (2000) 145.
[6] J. Zhao, C. Chen, W. Ma, Top. Catal. 35 (2005) 267.
[7] M. Anpo, Bull. Chem. Soc. Jpn. 77 (2004) 1427.
[8] D. Robert, Catal. Today 122 (2007) 20.
[9] C. Lettmann, H. Hinrichs, W.F. Maier, Angew. Chem. Int. Ed. 40 (2001) 3160.
[10] S. Malato, J. Blanco, A. Vidal, C. Richter, Appl. Catal. B-Environ. 37 (2002) 1.
[11] J. Liqiang, Q. Yichun, W. Baiqi, L. Shudan, J. Baojiang, Y. Libin, F. Wei, F. Honggang, S. Jiazhong, Sol. Energy Mater. Sol. Cells 90 (2006) 1773.
[12] A. Kubacka, M. Fernández-García, G. Colón, J. Catal. 254 (2008) 272.
[13] E. Gkika, A. Troupis, A. Hiskia, E. Papaconstantinou, Appl. Catal. B-Environ. 62 (2006) 28.

[14] E. Gkika, P. Kormali, S. Antonaraki, D. Dimoticali, E. Papaconstantinou, A. Hiskia, Int. J. Photoenergy 6 (2004) 227.
[15] D. Chatterjee, S. Dasgupta, J. Photochem. Photobiol. C 6 (2005) 186.
[16] A. Kudo, H. Kato, I. Jsuji, Chem. Lett. 33 (2004) 1534.
[17] L. Zhou, W. Wang, L. Zhang, H. Xu, W. Zhu, J. Phys. Chem. C 111 (2007) 13659.
[18] L. Zhang, D. Chen, X. Jiao, J. Phys. Chem. B 110 (2006) 2668.
[19] X. Hu, C. Hu, J. Qu, Mater. Res. Bull. 43 (2008) 2986.
[20] S.T. Lim, T.W. Kim, S.G. Hur, S.J. Hwang, H. Park, W. Choi, J.H. Choy, Chem. Phys. Lett. 434 (2007) 251.
[21] S. Zhu, T. Xu, H. Fu, J. Zhao, Y. Zhu, Environ. Sci. Technol. 41 (2007) 6234.
[22] J. Tang, Z. Zou, J. Ye, Angew. Chem. Int. Ed. 43 (2004) 4463.
[23] M. Oshikiri, M. Boero, J. Ye, Z. Zou, G. Kido, J. Chem. Phys. 117 (2002) 7313.
[24] H. Liu, R. Nakamura, Y. Nakato, J. Electrochem. Soc. 152 (2005) G856.
[25] R. Machado, M.G. Stachiotti, R.L. Migoni, A.H. Tera, Phys. Rev. B 70 (2004) 214112.
[26] B. Muktha, T. Aarthi, G. Madras, T.N. Guru Row, J. Phys. Chem. B 110 (2006) 10280.
[27] S. Matsushima, K. Obata, H. Nakamura, M. Arai, K. Kobayashi, J. Phys. Chem. Solids 64 (2003) 2417.
[28] A. Martínez-de la Cruz, S. Obregón Alfaro, E. López Cuéllar, U. Ortiz Méndez, Catal. Today 129 (2007) 194.
[29] L. Wu, J. Bi, Z. Li, X. Wang, X. Fu, Catal. Today 131 (2008) 15.
[30] H. Fu, C. Pan, L. Zhang, Y. Zhu, Mater. Res. Bull. 42 (2007) 696.
[31] S. Zhang, J. Shen, H. Fu, W. Dong, Z. Zheng, L. Shi, J. Solid State Chem. 180 (2007) 1456.
[32] M.P. Pechini, N. Adams, US Patent 3,330,697 (1967).
[33] Joint Committee on Powder Diffraction Standards, The International Centre for Diffraction Data (ICDD) Campus Blvd., Newtown Square, PA 19073-3273 U.S.A.
[34] T.J.B. Holland, S.A.T. Redfern, Mineral. Mag. 61 (1997) 65.
[35] A.D. Rae, J.G. Thompson, R.L. Withers, Acta Crystallogr. B 47 (1991) 870.
[36] Y. Shimodaira, H. Kato, H. Kobayashi, A. Kudo, J. Phys. Chem. B 110 (2006) 17790.
[37] K.S. Knight, Mineral. Mag. 56 (1992) 399.
[38] J. Tang, Z. Zhou, J. Yin, J. Ye, Catal. Lett. 92 (2004) 53.
[39] G. Colón, C. Belver, M. Fernández-García, in: J.A. Rodríguez, M. Fernández-García (Eds.), Synthesis, Properties, and Applications of Oxide Nanomaterials, John Wiley & Sons, New Jersey, 2007 (Chapter 17).
[40] A. Kudo, I. Tsuji, H. Kato, Chem. Commun. (2002) 1958.
[41] M.A. Butler, J. Appl. Phys. 48 (1977) 1914.
[42] J. Tauc, Mater. Res. Bull. 5 (1970) 721.
[43] H. Fu, C. Pan, W. Yao, Y. Zhu, J. Phys. Chem. B 109 (2005) 22432;
H. Fu, L. Zhang, W. Yao, Y. Zhu, Appl. Catal. B-Environ. 66 (2006) 100.
[44] J. Bi, L. Wu, J. Li, Z. Li, X. Wang, X. Fu, Acta Mater. 55 (2007) 4699.
[45] J. Ryu, W. Choi, K.H. Choo, Water Sci. Technol. 51 (2005) 491.
[46] N. Serpone, J. Photochem Photobiol. A 104 (1997) 1.
[47] T. Wu, G. Liu, J. Zhao, H. Hidaka, N. Serpone, J. Phys. Chem. B 102 (1998) 5845.
[48] P. Qu, J. Zhao, T. Shen, H. Hidaka, J. Mol. Catal. A-Chem. 129 (1998) 257.